RESEARCH ARTICLE

Reproducibility and usefulness of quantitative apparent diffusion coefficient measurements for predicting program death-ligand 1 expression in nasopharyngeal carcinoma

Xi Zhong[1†], Li Li[2†], Jinxue Yin[1†], Yuanlin Chen[3], Xin Xin[1], Lanlan Yu[1], Yongfang Tang[1], Jiangyu Zhang[3*] and Jiansheng Li[1*]

Abstract

Background Accurate assessment of programmed death-ligand 1 (PD-L1) expression status in nasopharyngeal carcinoma (NPC) before immunotherapy is crucial. We aimed to explore the reproducibility and usefulness of the quantitative apparent diffusion coefficient (ADC) measurements for predicting PD-L1expression status in NPC.

Methods We retrospectively recruited 134 NPC patients who underwent MRI scans and PD-L1 detection. A PD-L1 combined positive score (CPS) ≥ 20 was identified as high expression status. Patients were divide into two cohorts based on the MRI scanning devices, including a 1.5-T MRI cohort (n = 85, 44 PD-L1 high expression) and a 3.0-T MRI cohort (n = 49, 24 PD-L1 high expression). The mean ADC (ADC_{mean}), minimum ADC (ADC_{min}) and maximal ADC (ADC_{max}) values were independently measured by two observers. The ADC measurement reproducibility was assessed by interclass correlation coefficients (ICC). The correlations between ADC parameters and CPS were analyzed by spearman's correlation coefficient (r), and the performance for PD-L1expression status prediction was assessed by the area under receiver operating characteristic curve (AUC).

Results The measurement reproducibility of ADC_{mean}, ADC_{min} and ADC_{max} was good in the 1.5-T MRI cohort (ICC: 0.843–0.930) and 3.0-T MRI cohort (ICC: 0.929–0.960). The ADC_{mean}, ADC_{min}, and ADC_{max} tended to inversely correlate with the CPS (r:-0.37 - -0.52 in the 1.5-T MRI cohort, and − 0.52 - -0.60 in the 3.0-T MRI cohort; *P* all < 0.01). The ADC_{mean}, ADC_{min} and ADC_{max} yielded the AUC of 0.756 (95% CI: 0.651, 0.861), 0.689 (95% CI: 0.576, 0.802), and 0.733 (95%CI: 0.626, 0.839) in the 1.5-T MRI cohort and 0.820 (95%CI: 0.703, 0.937), 0.755 (95% CI: 0.616, 0.894), and 0.760 (95%CI: 0.627, 0.893) in the 3.0-T MRI cohort for predicting PD-L1 high expression status, respectively.

---

†Xi Zhong, Li Li and Jinxue Yin contributed equally to this work.

*Correspondence:
Jiangyu Zhang
Superchina2000@foxmail.com
Jiansheng Li
lijiansheng@gzhmu.edu.cn

Full list of author information is available at the end of the article

Conclusion ADC measurements may act as a reproducible and feasible method to predict PD-L1 expression status in NPC.

Keywords Nasopharyngeal carcinoma, Programmed death ligand 1, Magnetic resonance imaging, Apparent diffusion coefficients

Background

Nasopharyngeal carcinoma (NPC) mortality rate was over 130,000 cases per year, and nearly 50% of NPC cases occurred in South China [1]. Approximately 10% of NPC patients developed distant metastasis at initial diagnosis, and 25% of patients developed recurrence or metastasis within 5 years after chemoradiotherapy [2]. Systemic chemotherapy has been proposed as a standard therapeutic strategy for NPC patients with recurrence or distant metastasis, but the treatment effect was frequently unsatisfactory, novel treatment strategies for advanced NPC are urgently needed [3].

Immunotherapy with checkpoint blockade inhibitors, especially programmed cell death protein-1/programmed cell death ligand 1 (PD-1/PD-L1) blockades, have shown broad application for advanced cancer therapy, such as head and neck squamous cell carcinoma (HNSCC), lung cancer, melanoma, and esophageal cancer [4–7]. For advanced NPC, clinical trial results have demonstrated that PD-1/PD-L1 blockades have significantly improved patient outcomes compared with traditional systemic chemotherapy [8, 9]. The PD-L1 status is a stratification factor for ongoing clinical trials for NPC. The immunotherapy response rate for NPC patients with high PD-L1 expression was higher than patients with low PD-L1 expression. However, the role of high PDL1 in predicting response to immunotherapy remains controversial [8–10]. The unclear predictive value of PD-L1 expression in NPC may be partly attributed to the PD-L1 detection approach. Currently, immunohistochemistry (IHC) is the most common approach for detecting PD-L1 expression in clinical practice. There are some shortcomings for PD-L1 detection in NPC, such as the tissue used for PD-L1 measurement is usually based on invasive aspiration biopsy. In addition, if the punctured NPC tissue is not enough, it may be difficult to precisely reflect the PD-L1 status due to increased tumor heterogeneity. Thus, it is important to seek an alternative quantitative method to noninvasively assess PD-L1 expression status.

Apparent diffusion coefficients (ADC) derived from diffusion-weighted imaging (DWI) could quantitatively reflect the structural and pathophysiological changes of tumors. ADC measurement is now widely applied in early diagnosis, chemoradiotherapy response evaluation and prognosis prediction in NPC [11–13]. Previous studies have demonstrated that ADC values have been significantly associated with HER-2 expression status in breast cancer, Ki-67 expression status in rectal adenocarcinoma and EGFR expression status in lung adenocarcinoma [14–16]. In addition, quantitative ADC parameters have shown potential values for predicting PD-L1 expression status in HNSCC [17] and brain metastases of lung cancer [18]. To our knowledge, the value of ADC for assessing PD-L1 expression in NPC remains unclear. Therefore, the present study aimed to explore the usefulness of ADC measurements for predicting PD-L1expression status in NPC.

Materials and methods

Patients

Ethical approval of the study protocol was obtained from the Ethics Review Board at Affiliated Cancer Hospital & Institute of Guangzhou Medical University, and the "waiver of informed consent" was approved by the Institutional Ethics Committee. Between January 2019 and June 2022, 213 consecutive patients confirmed with non-keratinizing differentiated or undifferentiated carcinoma (WHO classes II and III) NPC who underwent PD-L1 detection using immunohistochemistry staining were selected. Clinical features, laboratory findings, pathology and MRI data were retrospectively analyzed. The inclusion criteria were as follows: (1) nasopharyngeal MRI scan was performed within two weeks of pathological confirmation; (2) availability of complete clinical records, including patients' age, sex, TNM stage (AJCC 8th) and clinical stage. Patients with a history of adjuvant therapy before MRI were excluded. Based on inclusion and exclusion criteria, 79 patients were excluded due to the following reasons: (1) unavailability of MRI data (n=43); (2) incomplete clinical records (n=15); (3) underwent chemoradiotherapy before MRI (n=21). Finally, 134 patients (101 men, 33 women; 24 to 76 years old) were included, and patients were divide into two cohorts, including the 1.5-T MRI cohort (n=85, patients underwent at 1.5T MRI) and the 3.0-T MRI cohort (n=49, patients underwent at 3.0T MRI).

PD-L1 detection and classification of expression

PD-L1 detection was performed using standard immunohistochemical (IHC) staining methods, and the PD-L1 was examined in the samples taken from the primary NPC. Biopsied tumor specimens were fixed in formalin, and paraffin-embedded tissues were sectioned at 4-μm thickness. We used the Dako Auto stained link 48 automated slide stainer (PD-L1 22c3, Dako, USA) to stain the tumor sections with PD-L1 antibody according to

the recommended operator instructions. The immunostained tissue sections were scored by two independent pathologists (J.Y.Z, with 22 years and Y.L.C with 6 years of experience) who were blinded to the clinical data. The PD-L1 combined positive score (CPS) was calculated as follows: CPS = ([PD-L1 membrane staining positive tumor cells+PD-L1 membrane staining positive tumor-associated immune cells] / Total number of tumor cells) × 100.Disagreements on the assessment of CPS were resolved by consensus two weeks after the individual interpretations. PD-L1 high expression status was defined as CPS≥20, and CPS < 20 was identified as low PD-L1 expression [19].

Acquisition of MR images

A total of 85 patients underwent 1.5-T MRI (Philips Achieva) scans, and 49 patients underwent 3.0-T MRI (GE Discovery) scans. All MRI examinations were performed using a sixteen-channel head and neck coil, and the scanning range was from the skull base to the subclavian region. The imaging sequences were comprised of axial T1-weighted imaging (T1WI), axial T2-weighted imaging (T2WI), axial contrast-enhanced T1-weighted imaging (CE-T1WI), axial DWI (b=0, 800 s/mm2), coronal fat suppression T2WI and coronal CE-T1WI. Gadolinium (Gd-DTPA; Schering, Berlin, Germany) was applied for CE-T1WI, with a bolus dose of 0.1 mmol/kg. The ADC maps were automatically generated based on the monoexponential decay model as follows: ADC = $(-\ln S_b/$.

$S_0)$ /b, where b=800 s/mm^2 and S_0 was the signal intensity corresponding to no diffusion gradients (b=0 s/mm^2). Detailed information of the imaging parameters is shown in Table 1.

ADC measurements

The ADC measurements were independently performed on a post processing workstation by two radiologists (observer 1, X.Z with 8 years of image processing experience; observer 2, J.X.Y with 6 years of image processing experience). As shown in Fig. 1, regions of interest (ROIs) were manually positioned for each primary NPC on the section of the ADC maps that depicted the tumor maximum area to minimize the influence of a partial volume averaging effect. The regions of necrosis (obvious hyperintensity on T2-w images and unenhanced on enhanced T1-w images) were carefully avoided. As described in our previous study, three small ROIs with a similar area were drawn inside the lesion to minimize the selection bias of a single ROI measurement [20]. Then the mean ADC (ADC$_{mean}$), minimum ADC (ADC$_{min}$) and maximal ADC (ADC$_{max}$) for each ROI were calculated, and the ADC parameters calculated for the three ROIs were averaged. The inter-observer reproducibility of ADC measurements between the observer 1 and observer 2 were assessed by using interclass correlation coefficients (ICC), and ADC values measured by the two observers were averaged for analysis.

Statistical analyses

Data analyses were performed by using R statistical software (version 3.3.1, http://www.rproject.org/), and $P<0.05$ indicated statistical significance. Categorical variables were expressed as numbers (%); quantitative variables were expressed as mean and standard deviation. An independent t-test was used to compare the differences of ADC parameters, and Pearson's χ^2 test or Fisher's exact test was used for categorical variables. Spearman's correlation coefficient (r) was used to analyze correlations between ADC parameters and CPS. ROC analyses were applied to create the optimal cut-off ADC values for

Table 1 MRI sequences and parameters

MRI Sequences	b value (s/mm^2)	TR/TE (ms)	Gap (mm)	ST (mm)	FOV(cm)	Matrix	NEX
1.5T MRI examination							
Axial TSE T1-weighted	-	545/14	4	4	26×25	328×220	1
Axial TSE T2-weighted	-	3193/80	5	5	26×25	228×185	2
Coronal FS T2-weighted	-	3224/165	5	5	26×25	312×163	1
Axial contrast-enhanced TSE T1-weighted	-	545/14	4	4	26×25	252×219	1
Sagittal contrast-enhanced TSE T1-weighted	-	545/14	4	4	26×25	304×205	1
Axial diffusion-weighted imaging	0, 800	5500/70	2	5	26×25	100×180	2
3.0T MRI examination							
Axial TSE T1-weighted	-	575/20	5	5	26×25	256×192	2
Axial TSE T2-weighted	-	4000/90	5	5	26×25	256×192	2
Coronal FS T2-weighted	-	2470/68	5	5	26×25	256×256	1
Axial contrast-enhanced TSE T1-weighted	-	506/14	5	5	26×25	256×192	1
Sagittal contrast-enhanced TSE T1-weighted	-	506/14	5	5	26×25	256×192	1
Axial diffusion-weighted imaging	0, 800	6000/80	2	5	26×25	105×200	2

Abbreviations: *FS* fat suppression, *TR* repetition time, *TE* echo time, *ST* slice thickness, *FOV* field of view, *NEX* number of excitation
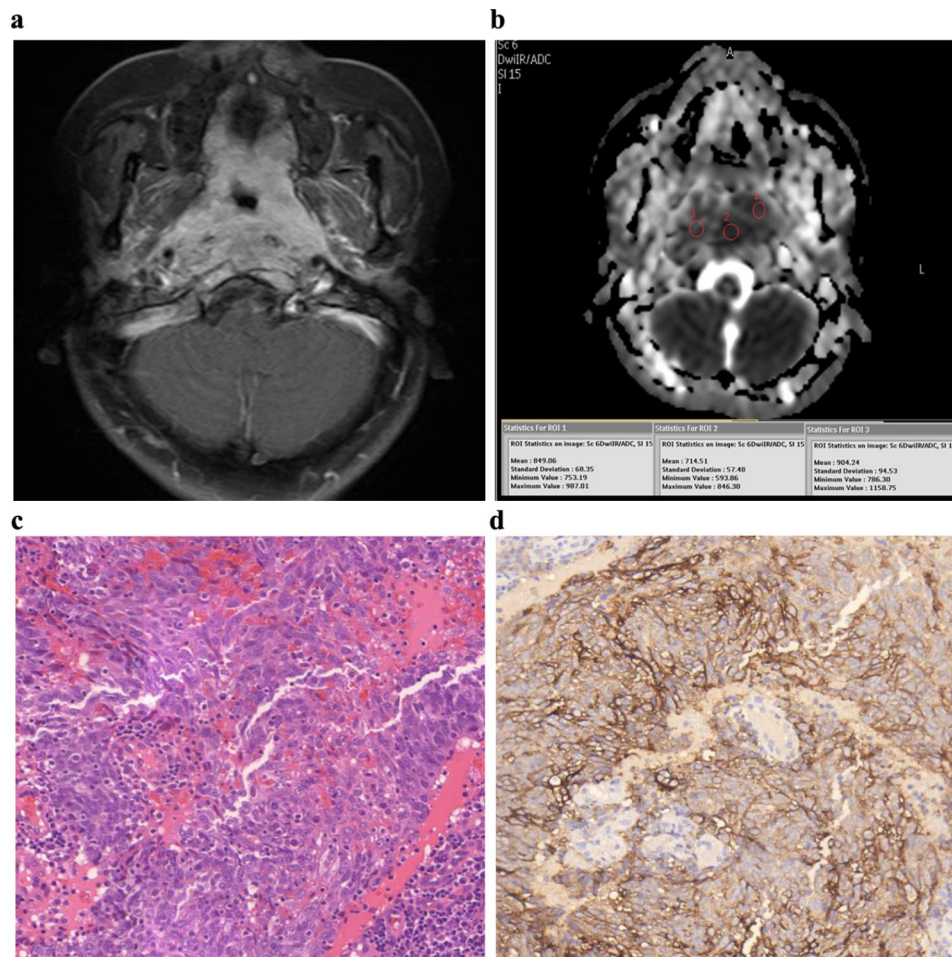
Fig. 1 ADC measurements for a 53-year-old female with NPC. (**a**) An obvious enhancement nasopharyngeal mass with skull base bone destruction is detected on enhanced T1-w image. (**b**) Three ROIs are manually placed inside the lesion on the ADC maps; the ADC_{mean}, ADC_{min} and ADC_{max} are documented. (**c**) Undifferentiated NPC is confirmed by HE staining pathology. (**d**) PD-L1 high expression status is determined by immunohistochemical (IHC) staining

predicting PD-L1 expression status, and the area under the ROC curves (AUC), sensitivity and specificity were calculated.

Results

Patient characteristics

Of the 134 patients enrolled in this study, 85 patients (n=44, high PD-L1 expression; n=41, low PD-L1 expression) that were evaluated with a 1.5-T MRI scan were assigned to the 1.5T MRI cohort, and 49 patients (n=24, high PD-L1 expression; n=25, low PD-L1 expression) that were examined with a 3.0-T MRI scan were assigned to the 3.0T MRI cohort. The frequency of patients with high PD-L1 expression showed no significant difference between the 1.5-T MRI cohort and 3.0-T MRI cohort (51.76% vs. 48.98%, *P*=0.756). Detailed patient characteristics are shown in Table 2.

The reproducibility of ADC measurements

The reproducibility of the ADC measurements between the two observers were very good. The ICC values of ADC_{mean}, ADC_{min} and ADC_{max} were 0.930 (95% CI: 0.894, 0.954), 0.880 (95% CI: 0.821, 0.920), and 0.843 (95% CI: 0.768, 0.891) in the 1.5-T MRI cohort and 0.960 (95% CI:0.930, 0.977), 0.929 (95% CI:0.877, 0.959), and 0.931 (95% CI:0.881, 0.961) in the 3.0-T MRI cohort, respectively.

Correlations between ADC parameters and PD-L1 combined positive score (CPS)

As shown in Fig. 2, the ADC_{mean}, ADC_{min} and ADC_{max} showed weak or moderate inverse correlation with the CPS (*P* all <0.01); the correlation coefficients (r) between the ADC_{mean}, ADC_{min}, ADC_{max} and CPS were −0.52, -0.37, and −0.48 in the 1.5-T MRI cohort (Fig. 2a-c), and

Table 2 Patients characteristics

Characteristics	1.5-T MRI cohort (n = 85)	3.0-T MRI cohort (n = 49)	P
PD-L1status (No. %)			0.756
High expression	44 (51.76%)	24 (48.98%)	
Low expression	41 (48.24%)	25 (51.02%)	
PD-L1 CPS (mean ± SD)	30.75 ± 26.28	37.65 ± 31.57	0.177
Age (mean ± SD)	50.53 ± 10.39	50.43 ± 13.36	0.961
Gender (No. %)			0.978
Male	64 (75.29%)	37 (75.51%)	
Female	21 (24.71%)	12 (24.49%)	
Histology, WHO type			0.729
II	46 (54.12%)	25 (51.02%)	
III	39 (45.88%)	24 (48.98%)	
T stage (No. %)			0.948
T1	7 (8.23%)	4 (8.16%)	
T2	21 (24.71%)	12 (24.49%)	
T3	38 (44.71%)	24 (48.98%)	
T4	19 (22.35%)	9 (18.37%)	
N stage (No. %)			0.79
N0	3 (3.53%)	2 (4.08%)	
N1	20 (23.53%)	14 (28.57%)	
N2	37 (43.53%)	17 (34.69%)	
N3	25 (29.41%)	16 (32.66%)	
M stage			0.783
M0	75 (88.24%)	44 (89.80%)	
M1	10 (11.76%)	5 (10.20%)	
Clinical stage			0.629
II	13 (15.29%)	4 (8.16%)	
III	32 (37.65%)	22 (44.90%)	
IVa	30 (35.30%)	18 (36.73%)	
IVb	10 (11.76%)	5 (10.21%)	

Abbreviations: *PD-L1* Programmed cell death ligand 1, *CPS* combined positive score

−0.60, -0.52, and −0.58 in the 3.0-T MRI cohort (Fig. 2d-f), respectively.

Performances of ADC parameters for predicting PD-L1 expression status

As displayed in Table 3, the ADC_{mean}, ADC_{min}, and ADC_{max} in PD-L1 high expression group were significantly lower than low expression group in the 1.5-T MRI cohort and 3.0-T MRI cohort (*P* all < 0.05). For predicting PD-L1 expression status, the ADC_{mean}, ADC_{min} and ADC_{max} yielded the AUC values of 0.756 (95% CI: 0.651, 0.861), 0.689 (95% CI: 0.576, 0.802), and 0.733 (95% CI: 0.626, 0.839) in the 1.5-T MRI cohort (Figs. 3) and 0.820 (95% CI: 0.703, 0.937), 0.755 (95% CI : 0.616, 0.894), and 0.760 (95% CI: 0.627, 0.893) in 3.0-T MRI cohort (Fig. 4), respectively.

As displayed in Table 4, the ADC_{mean} showed an optimal efficacy for predicting PD-L1 expression status. With the cut off value of $ADC_{mean} \le 864.00 \times 10^{-6} mm^2/s$, the ADC_{mean} yielded a sensitivity of 81.82% and specificity

of 68.29% for predicting PD-L1 high expression in the 1.5-T MRI cohort. With the cut off value of $ADC_{mean} \le 876.00 \times 10^{-6} mm^2/s$, the ADC_{mean} yielded a sensitivity of 87.50% and specificity of 76.00% for predicting PD-L1 high expression status in the 3.0-T MRI cohort, respectively.

Discussion

In the present study, we investigated the reproducibility and usefulness of ADC measurements using 1.5-T and 3.0-T MRI for predicting PD-L1 expression status in NPC. The results indicated the reproducibility of ADC measurements were good for 1.5-T MRI and 3.0-T MRI cohort, and the ADC_{mean}, ADC_{min} and ADC_{max} values tended to inversely correlate with the PD-L1 expression. In addition, we found that the ADC_{mean} showed an optimal efficacy for predicting high PD-L1 expression status, which yielded the AUC of 0.756 and 0.820 in the 1.5-T MRI and 3.0-T MRI cohort, respectively. Thus, our results indicated that ADC measurements may act as a helpful strategy to noninvasively predict PD-L1 expression status in NPC.

At present, ADC measurements have shown to be a promising strategy for early diagnosis, chemotherapy response assessment and prognosis prediction in NPC [11–13]. However, the reproducibility of ADC measurements for NPC at different MRI systems is rarely assessed. In fact, the reproducibility of ADC measurements at different MRI systems should be assessed because ADC may be influenced by field strength [21, 22]. Ye et al. assessed the ADC reproducibility of pancreas measured with different MRI systems and demonstrated that ADC measurements of the pancreas may be affected by field strength, but showed good reproducibility for both 1.5 T and 3.0T MRI systems [22]. In the present study, we found that the ICC values of the ADC measurements ranged from 0.843 to 0.930 in the 1.5-T MRI cohort and 0.929 to 0.960 in the 3.0-T MRI cohort, which suggested that the ADC measurements at different MRI systems for NPC were reproducible.

The noninvasive assessment of tumor PD-L1 expression using modern imaging techniques has produced much attention. The irregular tumor margin and peritumoral low signal intensity on hepatobiliary phase images have been independently associated with PD-L1 expression in hepatocellular carcinoma, with an AUC of 0.809 for predicting high PD-L1 expression [23]. A prediction model that consisted of functional parameters derived from PET/CT and intravoxel incoherent motion (IVIM)-MRI showed effective performance for classifying PD-L1 expression in lung cancer, with the AUC of 0.946, sensitivity of 85.29% and specificity of 91.67% [24]. As for NPC, the tumor maximum standardized uptake value (SUV_{max}) measured with PET/CT was positively
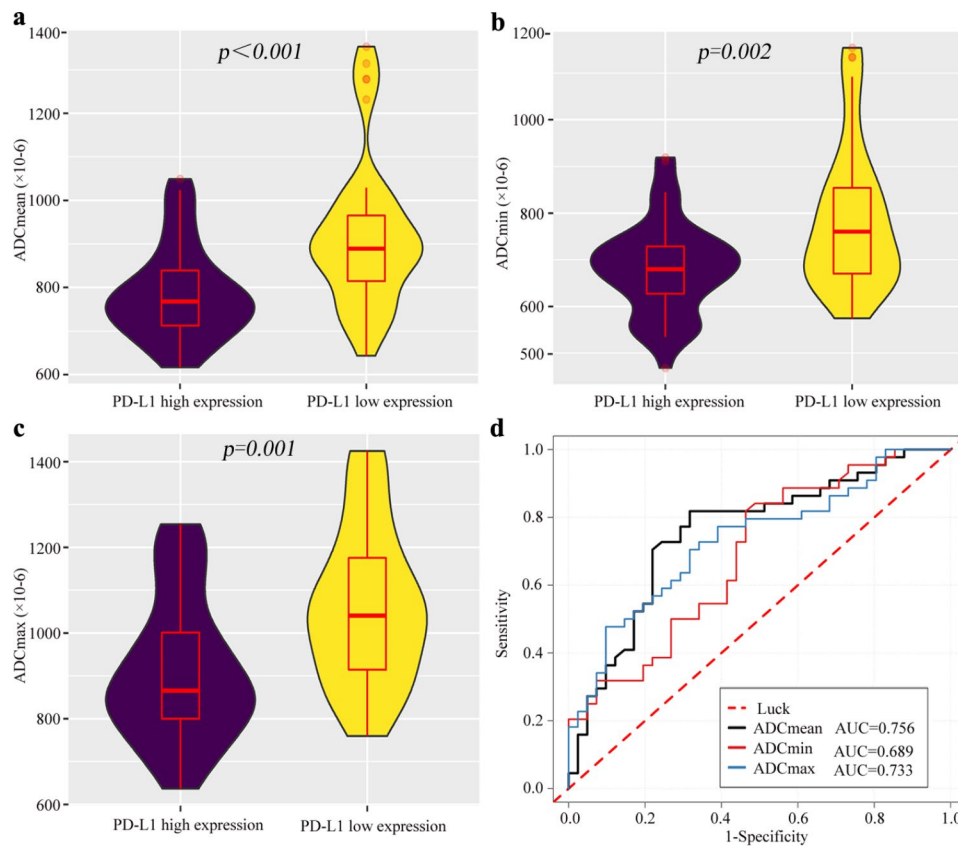
Fig. 2 Correlations between ADC parameters and PD-L1 expression. (**a-c**) The ADC_{mean}, ADC_{min} and ADC_{max} measured at 1.5-T MRI have a weak or moderate inverse correlation with the CPS, showing correlation coefficients (r) of -0.52, -0.370 and −0.48, respectively. (**b**) The ADC_{mean}, ADC_{min} and ADC_{max} measured at 3.0-T MRI have a moderate inverse correlation with the CPS, showing r of -0.60, -0.52 and −0.58, respectively

Table 3 Difference comparisons of ADC parameters between PD-L1 high expression and low expression

ADC parameters	1.5-T MRI cohort(n = 85)			3.0-T MRI cohort (n = 49)		
	PD-L1 high expression (n = 44)	PD-L1 low expression (n = 41)	P	PD-L1 high expression (n = 24)	PD-L1 low expression (n = 25)	P
ADC_{mean} ($\times 10^{-6}$ mm²/s)	786.68 ± 105.69	918.63 ± 169.87	<0.001	739.96 ± 129.34	923.66 ± 153.34	<0.001
ADC_{min} ($\times 10^{-6}$ mm²/s)	682.31 ± 99.28	786.09 ± 152.55	0.002	669.62 ± 157.09	827.70 ± 171.01	<0.001
ADC_{max} ($\times 10^{-6}$ mm²/s)	912.90 ± 164.69	1061.70 ± 180.89	0.001	853.17 ± 131.73	1015.40 ± 169.59	<0.001

Abbreviations: *ADC* apparent diffusion coefficient, ADC_{mean} Mean ADC, ADC_{min} Minimum ADC, ADC_{max} Maximal ADC

associated with PD-L1 expression in NPC, and yielded an AUC value of 0.733 for predicting high PD-L1 expression [25]. Thus, quantitative functional imaging may show potential value to non-invasively predict PD-L1 expression status in NPC.

In the present study, we found that ADC parameters were significantly negatively associated with PD-L1 expression in NPC. The correlation coefficients (r) between the ADC_{mean}, ADC_{min}, ADC_{max} and CPS ranged from −0.37 to -0.52 in the 1.5-T MRI cohort and −0.52 to -0.60 in the 3.0-T MRI cohort, respectively. Our findings were partly similar to the Meyer et al. study [17], in which 29 HNSCC patients who underwent 3.0-T MRI were recruited to explore the correlations between ADC values and PD-L1 expression and found that ADC values

(r=-0.38) and ADC_{max} (r=-0.35) were weakly correlated with PD-L1 immune cell score. In addition, Yilmaz et al. recruited 33 patients with brain metastases of lung cancer who underwent 1.5-T MRI to determine the relationships between ADC values and PD-L1 expression indicated that the ADC_{mean} in high PD-L1 expression metastases was significantly lower than in low PD-L1 expression metastases [18]. However, the performance of ADC parameters for predicting PD-L1 expression status in previous studies had not been analyzed due to the restricted number of samples.

The strength of this study was that the performances of ADC parameters for predicting PD-L1 expression status were analyzed in both the 1.5-T MRI cohort and 3.0-T MRI cohort. The results of our study demonstrated that
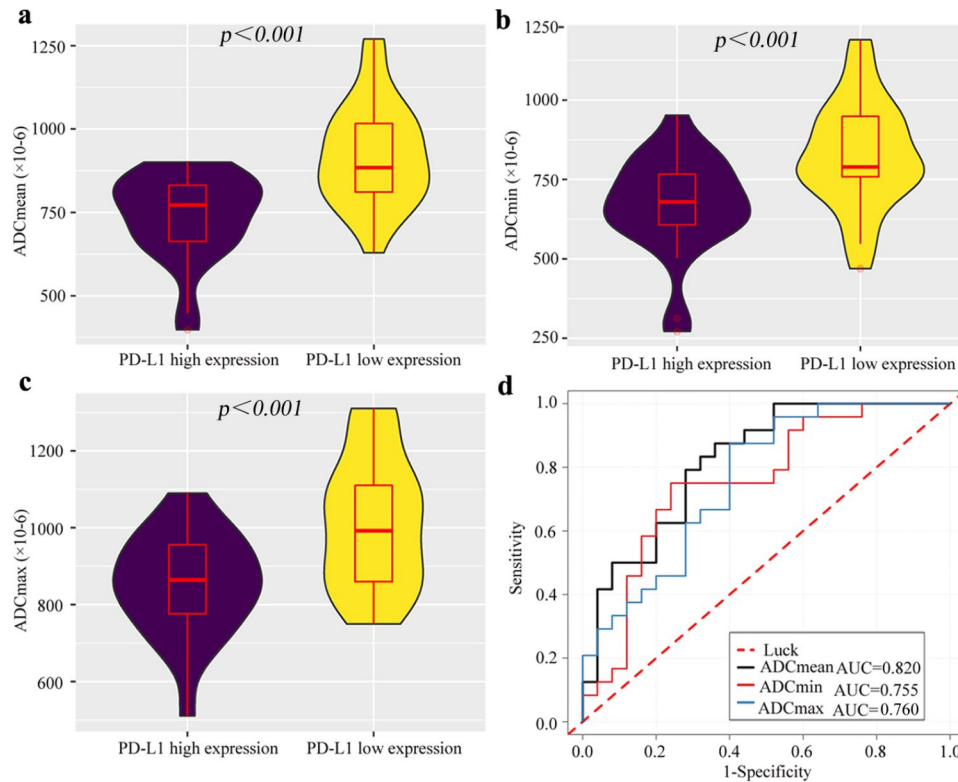
Fig. 3 The performances of ADC parameters for predicting PD-L1 expression status in the 1.5-T MRI cohort. The ADC_{mean} (**a**), ADC_{min} (**b**) and ADC_{max} (**c**) in PD-L1 high expression group is significantly lower than the low expression group (*P* all < 0.01). (**d**) ROC analysis of the ADC_{mean}, ADC_{min} and ADC_{max} for predicting high PD-L1 expression status, with the AUC values of 0.756, 0.689 and 0.733, respectively
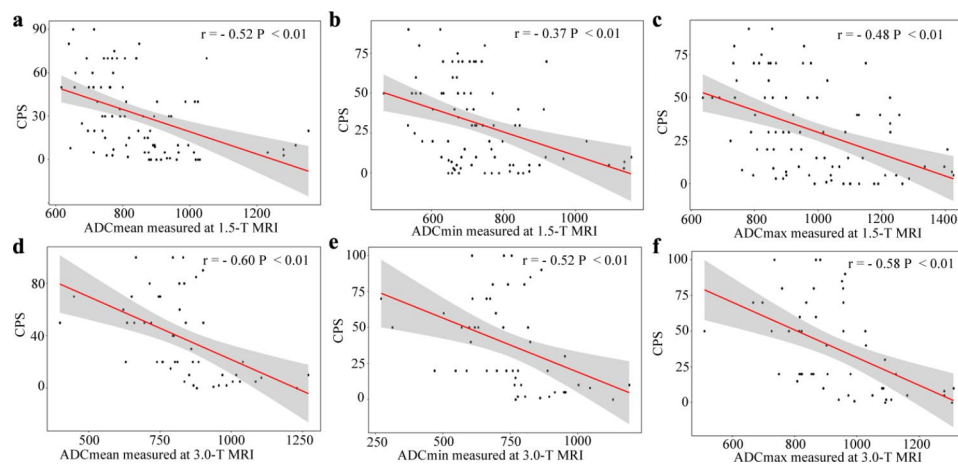

Fig. 4 The performances of ADC parameters for predicting PD-L1 expression status in the 3.0-T MRI cohort. The ADC_{mean} (**a**), ADC_{min} (**b**) and ADC_{max} (**c**) in PD-L1 high expression group is significantly lower than low expression group (*P* all < 0.01). (**d**) ROC analysis of the ADC_{mean}, ADC_{min} and ADC_{max} for predicting high PD-L1 expression status, with AUC values of 0.820, 0.755 and 0.760, respectively

the ADC_{mean}, ADC_{min} and ADC_{max} yielded AUC values that ranged from 0.689 to 0.756 in 1.5-T MRI cohort and 0.755 to 0.820 in 3.0-T MRI cohort for predicting PD-L1 high expression status. Furthermore, compared with ADC_{min} and ADC_{max}, we found that the ADC_{mean} showed an optimal efficacy, which yielded a sensitivity of 81.82% and specificity of 68.29% in the 1.5-T MRI cohort and a sensitivity of 87.50% and specificity of 76.00% in the 3.0-T MRI cohort, respectively. Thus, our results indicated that ADC parameters, especially the ADC_{mean} may act as feasible imaging biomarkers to noninvasively predict PD-L1 expression status in NPC.

Our study has several limitations. First, the study was a single-center and retrospective study with limited sample

Table 4 Performance evaluation of ADC parameters for predicting PD-L1 expression status

ADC parameters	AUC(95% CI)	Cut off value	Sensitivity	Specificity
1.5-T MRI cohort				
ADC_{mean} ($\times10^{-6}$ mm^2/s)	0.756 (0.651, 0.861)	864.00	81.82% (36/44)	68.29% (28/41)
ADC_{min} ($\times10^{-6}$ mm^2/s)	0.689 (0.576, 0.802)	747.00	84.09% (37/44)	53.66% (22/41)
ADC_{max} ($\times10^{-6}$ mm^2/s)	0.733 (0.626, 0.839)	971.00	77.27% (34/44)	68.29% (28/41)
3.0-T MRI cohort				
ADC_{mean} ($\times10^{-6}$ mm^2/s)	0.820 (0.703, 0.937)	876.00	87.50% (21/24)	76.00% (17/25)
ADC_{min} ($\times10^{-6}$ mm^2/s)	0.755 (0.616, 0.894)	758.00	75.00% (18/24)	76.00% (19/25)
ADC_{max} ($\times10^{-6}$ mm^2/s)	0.760 (0.627, 0.893)	1027.00	87.50% (21/24)	60.00% (15/25)

Abbreviations: *ADC* apparent diffusion coefficient, *ADC*$_{mean}$ Mean ADC, *ADC*$_{min}$ Minimum ADC, *ADC*$_{max}$ Maximal ADC, *AUC* area under the ROC curve

size, and a future multicentered study with a larger sample size is needed to verify the results generated. Second, as reported in a previous study [19], we adopted CPS≥20 as a cut-off value of high PD-L1 expression status. However, the optimal cut-off value of high PD-L1 expression in clinical practice for NPC remains unclear. Therefore, a multicenter, large sample prospective study should be carried out to compare the predictive performances of the different CPS cut-off values and seek the optimal and normalized cut-off value in predicting immunotherapy response. However, due to the potential relationships of ADC values with PD-L1 expression revealed in this study, the correlates of ADC values with immunotherapy response should be assessed in further studies. Third, PDL1 expression detection was based on biopsied tissue, and ADC-based testing was based on the whole solid tumor. Because of the high heterogeneity in PDL1 expression, the detection of PDL1 expression may not precisely reflect the true expression of the whole solid tumor, thus selection bias may be difficult to completely avoid in this study. Finally, the number of samples in the 3.0-T MRI cohort was obviously less than the 1.5-T MRI cohort, thus the performances of ADC parameters for predicting PD-L1 expression status between 1.5-T MRI cohort and 3.0-T MRI cohort were not compared.

Conclusion

The ADC_{mean}, ADC_{min} and ADC_{max} measurements at 1.5-T MRI and 3.0-T MRI for NPC were reproducible, and these ADC parameters showed potential value for predicting PD-L1 expression status. Thus, ADC measurements may act as a reproducible and feasible method to predict PD-L1 expression status in NPC.

Abbreviations

NPC	Nasopharyngeal carcinoma
PD-L1	Programmed cell death ligand 1
DWI	Diffusion-weighted imaging
ADC	Quantitative apparent diffusion coefficients
ADC_{mean}	Mean ADC
ADC_{min}	Minimum ADC
ADC_{max}	Maximal ADC
ROC	Receiver operating characteristic
AUC	Area under the receiver operating characteristic curve
ICC	Interclass correlation coefficients
ROI	Regions of interest
CPS	Combined positive score

Supplementary Information

The online version contains supplementary material available at https://doi.org/10.1186/s40644-023-00587-2.

> Supplementary Material 1
>
> Supplementary Material 2

Authors' contributions
Jiansheng Li, Xi Zhong and Jiangyu Zhang designed the study, performed most of the investigations, and data analysis. Li Li, Jinxue Yin and Yuanlin Chen contributed significantly to analysis and manuscript preparation. Xi Zhong and Xin Xin provided data and wrote the manuscript. Lanlan Yu and Yongfang Tang reviewed and edited the manuscript. All authors read and approved the manuscript.

Data Availability
The datasets used and/or analyzed during the current study available from the corresponding author on reasonable request.

Declarations

Ethics approval and consent to participate
The Institutional Review Board of Affiliated Cancer Hospital & Institute of Guangzhou Medical University approved this retrospective study and waived the requirement for written informed consent due to its retrospective nature.

Consent for publication
Not applicable.

Competing interests
The authors declare that they have no competing interests.

Author details
[1]Department of Medical Imaging, Affiliated Cancer Hospital & Institute of Guangzhou Medical University, Guangzhou 510095, China [2]Department of Otolaryngology, The Third Affiliated Hospital of Guangzhou Medical University, Guangzhou 510150, China [3]Department of Pathology, Affiliated Cancer Hospital & Institute of Guangzhou Medical University, Guangzhou 510150, China

Zhong *et al. Cancer Imaging*   (2023) 23:98

Page 9 of 9

References

1. Sung H, Ferlay J, Siegel RL, Laversanne M, Soerjomataram I, Jemal A, et al. Global Cancer Statistics 2020: GLOBOCAN estimates of incidence and Mortality Worldwide for 36 cancers in 185 countries. CA Cancer J Clin. 2021;71:209–49.
2. Lv X, Cao X, Xia WX, Liu KY, Qiang MY, Guo L, et al. Induction chemotherapy with lobaplatin and fluorouracil versus cisplatin and fluorouracil followed by chemoradiotherapy in patients with stage III-IVB nasopharyngeal carcinoma: an open-label, non-inferiority, randomised, controlled, phase 3 trial. Lancet Oncol. 2021;22:716–26.
3. Lee AW, Ma BB, Ng WT, Chan AT. Management of nasopharyngeal carcinoma: current practice and future perspective. J Clin Oncol. 2015;33:3356–64.
4. Larkins E, Blumenthal GM, Yuan W, He K, Sridhara R, Subramaniam S, et al. FDA approval Summary: Pembrolizumab for the treatment of recurrent or metastatic Head and Neck squamous cell carcinoma with Disease Progression on or after platinum-containing chemotherapy. Oncologist. 2017;22:873–8.
5. Fehrenbacher L, Spira A, Ballinger M, Kowanetz M, Vansteenkiste J, Mazieres J, et al. Atezolizumab versus docetaxel for patients with previously treated non-small-cell lung cancer (POPLAR): a multicentre, open-label, phase 2 randomised controlled trial. Lancet. 2016;387:1837–46.
6. Ribas A, Hamid O, Daud A, Hodi FS, Wolchok JD, Kefford R, et al. Association of Pembrolizumab with Tumor Response and Survival among patients with Advanced Melanoma. JAMA. 2016;315:1600–9.
7. Kato K, Cho BC, Takahashi M, Okada M, Lin CY, Chin K, et al. Nivolumab versus chemotherapy in patients with advanced oesophageal squamous cell carcinoma refractory or intolerant to previous chemotherapy (ATTRACTION-3): a multicentre, randomised, open-label, phase 3 trial. Lancet Oncol. 2019;20:1506–17.
8. Fang W, Yang Y, Ma Y, Hong S, Lin L, He X, et al. Camrelizumab (SHR-1210) alone or in combination with gemcitabine plus cisplatin for nasopharyngeal carcinoma: results from two single-arm, phase 1 trials. Lancet Oncol. 2018;19:1338–50.
9. Wang FH, Wei XL, Feng J, Li Q, Xu N, Hu XC, et al. Efficacy, Safety, and correlative biomarkers of Toripalimab in previously treated recurrent or metastatic nasopharyngeal carcinoma: a phase II clinical trial (POLARIS-02). J Clin Oncol. 2021;39:704–12.
10. Ma B, Lim WT, Goh BC, Hui EP, Lo KW, Pettinger A, et al. Antitumor Activity of Nivolumab in recurrent and metastatic nasopharyngeal carcinoma: an International, Multicenter Study of the Mayo Clinic Phase 2 Consortium (NCI-9742). J Clin Oncol. 2018;36:1412–8.
11. Ai QY, King AD, Chan J, Chen W, Chan KCA, Woo JKS, et al. Distinguishing early-stage nasopharyngeal carcinoma from benign hyperplasia using intravoxel incoherent motion diffusion-weighted MRI. Eur Radiol. 2019;29:5627–34.
12. Chen Y, Liu X, Zheng D, Xu L, Hong L, Xu Y, et al. Diffusion-weighted magnetic resonance imaging for early response assessment of chemoradiotherapy in patients with nasopharyngeal carcinoma. Magn Reson Imaging. 2014;32:630–7.
13. Liu LT, Guo SS, Li H, Lin C, Sun R, Chen QY, et al. Percent change in apparent diffusion coefficient and plasma EBV DNA after induction chemotherapy identifies distinct prognostic response phenotypes in advanced nasopharyngeal carcinoma. BMC Cancer. 2021;21:1320.
14. Meng N, Wang X, Sun J, Han D, Bai Y, Wei W, et al. A comparative study of the value of amide proton transfer-weighted imaging and diffusion kurtosis imaging in the diagnosis and evaluation of breast cancer. Eur Radiol. 2021;31:1707–17.
15. Li L, Chen W, Yan Z, Feng J, Hu S, Liu B, et al. Comparative analysis of Amide Proton transfer MRI and diffusion-weighted imaging in assessing p53 and Ki-67 expression of rectal adenocarcinoma. J Magn Reson Imaging. 2020;52:1487–96.
16. Meng N, Fu F, Feng P, Li Z, Gao H, Wu Y, et al. Evaluation of Amide Proton transfer-weighted imaging for Lung Cancer subtype and epidermal growth factor receptor: a comparative study with diffusion and metabolic parameters. J Magn Reson Imaging. 2022;56:1118–29.
17. Meyer HJ, Hohn AK, Surov A. Relationships between apparent diffusion coefficient (ADC) histogram analysis parameters and PD-L 1-expression in head and neck squamous cell carcinomas: a preliminary study. Radiol oncol. 2021;55:150–7.
18. Yilmaz TF, Yurtsever I, Turk HM, Gultekin MA, Besiroglu M, Cesme DH, et al. Relationship with programmed cell death ligand 1 (PD-L1) and DTI features in Brain Metastases of Non-small Cell Lung Cancer: a preliminary study. Curr Med Imaging. 2021;17:1369–73.
19. Saada-Bouzid E, Peyrade F, Guigay J. Immunotherapy in recurrent and or metastatic squamous cell carcinoma of the head and neck. Curr Opin Oncol. 2019;31:146–51.
20. Zhong X, Tang H, Guan T, Lu B, Zhang C, Tang D, et al. Added value of quantitative apparent diffusion coefficients for identifying small Hepatocellular Carcinoma from Benign Nodule categorized as LI-RADS 3 and 4 in cirrhosis. J Clin Transl Hepatol. 2022;10:34–41.
21. Ye XH, Gao JY, Yang ZH, Liu Y. Apparent diffusion coefficient reproducibility of the pancreas measured at different MR scanners using diffusion-weighted imaging. J Magn Reson Imaging. 2014;40:1375–81.
22. Kim SY, Lee SS, Byun JH, Park SH, Kim JK, Park B, et al. Malignant hepatic tumors: short-term reproducibility of apparent diffusion coefficients with breath-hold and respiratory-triggered diffusion-weighted MR imaging. Radiology. 2010;255:815–23.
23. Sun L, Mu L, Zhou J, et al. Imaging features of gadoxetic acid-enhanced MR imaging for evaluation of tumor-infiltrating CD8 cells and PD-L1 expression in hepatocellular carcinoma. Cancer Immunol Immunother. 2022;71:25–38.
24. Meng N, Fu F, Sun J, Tang W, Zhang L, Xie S, et al. Sensitivity and specificity of amide proton transfer-weighted imaging for assessing programmed death-ligand 1 status in non-small cell lung cancer: a comparative study with intravoxel incoherent motion and (18)F-FDG PET. Quant Imaging Med Surg. 2022;12:4474–87.
25. Zhao L, Zhuang Y, Fu K, Chen P, Wang Y, Zhuo J, et al. Usefulness of [(18)F]fluorodeoxyglucose PET/CT for evaluating the PD-L1 status in nasopharyngeal carcinoma. Eur J Nucl Med Mol Imaging. 2020;47:1065–74.

Publisher's Note

Springer Nature remains neutral with regard to jurisdictional claims in published maps and institutional affiliations.